Journal of Physiology (2002), **541.2**, *pp.* 467–482
DOI: 10.1113/jphysiol.2001.018333

www.jphysiol.org

Potassium channels Kv1.1, Kv1.2 and Kv1.6 influence excitability of rat visceral sensory neurons

Patricia A. Glazebrook *, Angelina N. Ramirez *, John H. Schild †, Char-Chang Shieh, Thanh Doan, Barbara A. Wible ‡ and Diana L. Kunze *

*Rammelkamp Center for Education and Research, MetroHealth Medical Center and Departments of *Neurosciences and ‡Biochemistry, Case Western Reserve University, Cleveland, OH 44109, USA and † Biomedical Engineering Program, IUPUI, Indianapolis, IN 46202, USA*

Voltage-gated potassium channels, Kv1.1, Kv1.2 and Kv1.6, were identified as PCR products from mRNA prepared from nodose ganglia. Immunocytochemical studies demonstrated expression of the proteins in all neurons from ganglia of neonatal animals (postnatal days 0–3) and in 85–90 % of the neurons from older animals (postnatal days 21–60). In voltage clamp studies, α-dendrotoxin (α-DTX), a toxin with high specificity for these members of the Kv1 family, was used to examine their contribution to K^+ currents of the sensory neurons. α-DTX blocked current in both A- and C-type neurons. The current had characteristics of a delayed rectifier with activation positive to −50 mV and little inactivation during 250 ms pulses. In current-clamp experiments α-DTX, used to eliminate the current, had no effect on resting membrane potential and only small effects on the amplitude and duration of the action potential of A- and C-type neurons. However, there were prominent effects on excitability. α-DTX lowered the threshold for initiation of discharge in response to depolarizing current steps, reduced spike after-hyperpolarization and increased the frequency/pattern of discharge of A- and C-type neurons at membrane potentials above threshold. Model simulations were consistent with these experimental results and demonstrated how the other major K^+ currents function in response to the loss of the α-DTX-sensitive current to effect these changes in action potential wave shape and discharge.

(Resubmitted 5 February 2002; accepted 5 March 2002)
Corresponding author D. L. Kunze: Rammelkamp Center R326, MetroHealth Systems, 2500 MetroHealth Drive, Cleveland, OH 44109-1998, USA. Email: dkunze@metrohealth.org

Visceral sensory neurons maintain resting potentials near −50 to −60 mV and are normally silent until they receive input from their peripheral sensory terminals (Jaffe & Sampson, 1976; Belmonte & Gallego, 1983; Stansfeld & Wallis, 1985; Ducreux *et al.* 1993). These cells are unipolar with a single parent axon exiting the soma and forming a 'T' as one branch passes centrally and the other peripherally. Thus, an action potential generated at the peripheral receptor invades the soma as well as passing directly to the central nervous system (Leiberman, 1976). Under most physiological conditions, the electrical properties of the somal membrane allow the soma to respond to each invading action potential without additional discharge that might feed back into the branches, altering the coding of the peripheral sensory information as it projects to the brainstem (Jaffe & Sampson, 1976; Gallego & Eyzaquirre, 1978; Stansfeld & Wallis, 1985). The faithful representation of the peripheral discharge at the soma can also be seen as a means of allowing processes within the soma to adjust expression of relevant proteins to match the needs of the active terminal in an activity-dependent manner (Devor, 1999).

We have been concerned with the identity and characteristics of the potassium channels that help stabilize the soma membrane potential following an invading action potential to minimize the risk of repetitive discharge. Our previous studies predicted a role for rapidly activating, slowly inactivating, 4-aminopyridine (4-AP)-sensitive potassium current in minimizing excitability of both A- and C-type neurons in response to depolarization (Schild *et al.* 1994). The electrical properties of the α-dendotoxin (α-DTX)-sensitive potassium channels, Kv1.1, Kv1.2 and Kv1.6, are similar to those expected of the current in our model with regard to threshold, activation time constant (τ) and slow inactivation (Christie *et al.* 1989; Stuhmer *et al.* 1989; Bertoli *et al.* 1994; Sprunger *et al.* 1996; D'Adamo *et al.* 1999). Furthermore, block of such a current by α-DTX had been reported to induce spontaneous discharge in myelinated sensory neurons (Stansfeld *et al.* 1986). The purpose of this study was to resolve the presence of these channels and assess their contributions to the activity of the visceral sensory neurons.

METHODS

Isolation and culture of ganglia

Nodose ganglia were excised from neonatal (postnatal days 0–3) or older (postnatal days 21–60) Sprague-Dawley rats. Tissue was collected from neonatal rats following asphyxiation by CO_2 inhalation and from older animals under halothane anaesthesia followed by decapitation in compliance with the Case Western Reserve University Animal Research Committee guidelines. All of the protocols employed in the labelling and harvesting of the ganglia have been approved by the Animal Research Committee. The neonatal ganglia were incubated in Earle's Balanced Saline Solution (EBSS) containing 5 mg ml^{-1} trypsin, 0.2 mg ml^{-1} cysteine, 0.5 mM EDTA and 1.5 mM $CaCl_2$, for 30 min at 37 °C. For older animals, the ganglia were placed in EBSS containing 1 mg ml^{-1} collagenase and incubated for 1 h at 37 °C. The enzyme-containing medium was then replaced with 3 ml of Dulbecco's modified Eagle's medium/F-12 with 5 % fetal bovine serum, 0.1 % serum extender, 100 U ml^{-1} penicillin, 100 μg ml^{-1} streptomycin and 1.5 mg ml^{-1} albumin. The tissue was triturated to disperse the cells and subsequently placed into 35 mm Petri dishes containing poly-D-lysine-treated glass coverslips.

Identification of specific populations of sensory neurones

To identify aortic baroreceptor neurons, the aortic depressor nerve was labelled with the fluorescent anterograde tracer Cell Tracker CM-DiI (Molecular Probes). Two- to three-week-old (30–75 g) Sprague-Dawley rats were anaesthetized with 1.2 ml kg^{-1} of a mixture of ketamine HCl (100 mg ml^{-1}), xylazine (20 mg ml^{-1}, Phoenix Pharmaceutical, Inc.) and acepromazine maleate (10 mg ml^{-1}) at a ratio of 1 : 1 : 2. The left aortic depressor nerve was identified caudal to joining the superior laryngeal nerve, freed from surrounding tissue for 3–4 mm and placed on a section of parafilm. Crystals of the tracer were applied to the uncut nerve and the region embedded with a fast-hardening compound, Kwik-Sil (World Precision Instruments). The surgical area was closed and the animal allowed to recover for 5–7 days. In a similar manner, the superior laryngeal nerve was labelled peripheral to the region where it joined the left aortic depressor nerve before entering the nodose ganglion and central to its division to external and internal branches.

PCR amplification of nodose ganglia K^+ channel subunit cDNA fragments

Nodose ganglia and brains from adult rats (6–8 weeks old) were excised and stored at –70 °C. mRNA was isolated using the MicroPoly(A)Pure kit (Ambion) following the manufacturer's instructions. Poly-(A^+) mRNA was quantitated by spectrophotometric absorbance at 260 nm and stored in aliquots at −80 °C.

Primer design. Sets of specific primers were designed to amplify unique DNA fragments corresponding to regions of rat Kv1.1, Kv1.2, Kv1.6, Kvβ1.1, Kvβ1.3, Kvβ2 and Kvβ3 by reverse transcriptase polymerase chain reaction (RT-PCR). Primer sequences and locations in published cDNA sequences in GenBank of the National Center for Biotechnology Information were as follows: Kv1.1 (accession number M26161), 5′-GAAGAAGCTGAGTCGCACTTCTCCAG-3′ (sense primer; nucleotides 1082–1107) and 5′-TTAAACATCGGTCAGGAGCTTGCTC-3′ (antisense primer; 1522–1497); Kv1.2 (X16003), 5′-GTCATCCGGTTGGTAAGAGTCTTTAG-3′ (sense primer; 1445–1470) and 5′-GTGTTAGCCAAGGTACAGTTGGCTG-3′ (antisense primer; 2022–1998); Kv1.6 (X17621), 5′-CTAGTGCAACGTCACGAGCAGCAGC-3′ (sense primer; 1376–1397) and 5′-AAGTGACGTGGGTATACTGGCCTTG-3′ (antisense primer; 1877–1852); Kvβ1.1 (X70662), 5′-ATGCAAGTCTCCATAGCCTGCACAGAGC-3′ (sense primer; 332–359) and 5′-GTCATCAGCCGTTCAGCAACCTCATCTG-3′ (antisense primer; 627–654); Kvβ1.3, 5′-GACAACAGCAAGTTTAGAAAGCAGTC-3′ (sense primer) and 5′-GTCATCAGCCGTTCAGCAACCTCATCTG-3′ (antisense primer) (Kuryshev *et al.* 2001); Kvβ2 (X76724), 5′-ATCTACAGTACTCGGTATGGGAGTC-3′ (sense primer; 662–686) and 5′-GCCTCCATGATCTCCATGGAGC-3′ (antisense primer; 1163–1185); and Kvβ3 (X76723), 5′-ATGCAGGTGTCTATCGCGTGTAC-3′ (sense primer; 388–410) and 5′-AAGCCTCGCTCAGTTTCTGCC-3′ (antisense primer; 881–902).

RT-PCR. Poly-A^+ mRNA (100 ng) was heat denatured at 70 °C for 5 min and then reverse transcribed into first-strand cDNA using a mixture of random hexameric, unlabelled deoxynucleotides and MuLV Reverse Transcriptase (First-Strand cDNA Synthesis Kit, Perkin-Elmer) at 42 °C for 1 h. The first-strand cDNA products were used directly as templates for PCR amplification. PCR was performed with the Advantage PCR System (Clontech) as follows: Each PCR vessel contained 5 pmol each of the sense and antisense primers, 0.2 mM deoxynucleotides and one unit of AdvanTaq (Clontech) in a final volume of 25 μl. The amplifications were performed using the following cycling programme: one cycle (2 min at 95 °C); 35 cycles (15 s at 94 °C, 15 s at 55 °C, 1 min at 68 °C); one cycle (10 min at 72 °C). For Kvβ1.1, Kvβ1.3, Kvβ2 and Kvβ3 the reaction conditions were: one cycle (2 min at 95 °C); 35 cycles (15 s at 94 °C, 15 s at 50 °C, 1 min at 68 °C); one cycle (10 min at 72 °C). PCR products of Kv1.1, Kv1.2, Kv1.6, Kvβ1.1, Kvβ1.3, Kvβ2 and Kvβ3 were resolved by electrophoresis on 1.2 % agarose gels, and transferred to BrightStar-Plus nylon membranes (Ambion) as recommended by the manufacturer. Following transfer, the membranes were baked at 80 °C in a vacuum oven. Channel-specific PCR products were identified by hybridization to radiolabelled internal oligonucleotides specific for Kv1.1, Kv1.2 and Kv1.6. The internal oligonucleotides were as follows: Kv1.1 (5′-TAGCCCACTACAGGCAGGCTAATATC-3′; nucleotides 1428–1453); Kv1.2 (5′-GGAGACATGGTTCCAACTACCATTG-3′; 1694–1718); and Kv1.6 (5′-GGCAGATGACGTTGACTCGCTCTTC-3′; 1627–1651). For the Kvβ family, Kvβ1.1 and Kvβ1.3 subunit specific PCR products were identified by hybridization to a ^{32}P-labelled internal oligonucleotide, 5′-GTTTCGTGCTTGGGTCTTGGAACATGG-3′. This region is conserved in both subunits. For Kvβ2 and Kvβ3 subunits 5′-GAGGCCAGATCACAGATGAG-3′ (nucleotides 774–793) and 5′-GGCTCTCAGATCTCAGATGAGACAG-3′ (nucleotides 691–715), respectively, were used. Radiolabelling was accomplished with T4 Polynucleotide Kinase in the presence of [γ-^{32}P]ATP. After the blots were prehybridized in Ultrasensitive Hybridization Solution (Ambion) at 44 °C for 1 h, [^{32}P]-labelled probe (at 10^6 c.p.m. ml^{-1}) was added and hybridized at 44 °C for up to 16 h. After hybridization, the blots were washed first with 2 × SSC(150 mM NaCl, 15 mM sodium citrate)/0.1 % sodium dodecyl sulphate (SDS) at room temperature followed by a more stringent wash with 0.1 × SSC/0.1 % SDS at 44 °C. Blots were exposed to BioMaxMS film (Kodak) at −80 °C with an intensifying screen.

The presence of Kvβ1.2 in nodose ganglia was determined by Northern blot analysis, as follows. Poly(A^+) RNA (2 μg per lane) was electrophoresed on a 1.0 % agarose–formaldehyde gel and transferred to Bright-Star membranes (Ambion). The blot was hybridized to a ^{32}P riboprobe spanning the region encoding the N-terminal 79 residues of human Kvβ1.2. A T7 promoter sequence was engineered directly onto the end of the coding fragment using

the Lig'nScribe kit from Ambion and the riboprobe synthesized with the Strip-EZ T7 kit (Ambion). The blot was hybridized with probe (10^6 c.p.m. ml^{-1}) overnight at 44 °C in ULTRAhyb buffer (Ambion), washed at 50 °C in 0.1 × SSC, 0.1 % SDS, and exposed to BioMax MS film (Kodak) at – 70 °C with an intensifying screen.

Western blotting and immunocytochemistry

Antibodies. Two Kv1.1 antibodies were used: a mouse monoclonal antibody (Upstate Biotechnology) raised against a C-terminal peptide (residues 458–476) of rat Kv1.1 and a rabbit polyclonal Kv1.1 (Alomone Labs) raised against a fusion protein with sequence corresponding to residues 416–495. Two Kv1.2 antibodies were used: a rabbit polyclonal (Alomone Labs) raised against a GST fusion protein coupled to a C-terminal portion of rat Kv1.2 (amino acids 417–498) and a mouse monoclonal (Upstate Biotechnology) raised against a GST fusion protein coupled to amino acids 428–499 of rat Kv1.2. Two Kv1.6 antibodies were used: a mouse monoclonal antibody (Upstate Biotechnology) raised against a C-terminal peptide (residues 506–524) of rat Kv1.6 and a rabbit polyclonal antibody (Alomone Labs) raised against a GST fusion protein linked to residues 463–530.

Tissue lysates and Western blotting. Frozen adult nodose ganglia were homogenized in ten volumes of lysis buffer consisting of 1 % Triton X-100, 150 mM NaCl, 50 mM Tris (pH 7.5) and 1 mM EDTA containing freshly added protease inhibitor. The homogenate was incubated on ice for 1 h and then centrifuged at 3000 *g* for 10 min and the insoluble debris discarded. The protein concentration of the lysate was measured by the BCA method (Pierce Chemical Co.). For rat brain, a crude membrane preparation was made by homogenization in five volumes of buffer consisting of 0.3 M sucrose, 10 mM $NaPO_4$, pH 7.2, and freshly added protease inhibitor cocktail. Following the removal of insoluble protein, the membrane preparation was centrifuged at 50 000 *g* for 1 h. The crude membrane fraction was resuspended in a small amount of homogenization buffer and the protein concentration was determined. Equal amounts of protein (50 μg) were separated on 8.5 % polyacrylamide SDS gels and transferred to PVDF membranes. The PVDF membranes were blocked with 5 % non-fat dry milk in PBS–0.1 % Tween-20 (PBS-T, Fisher Scientific) overnight at 4 °C and then incubated with primary antibodies mAb Kv1.1, mAb Kv1.2 and pAb Kv1.6. After washing, the blots were incubated for 1 h at room temperature with anti-mouse or anti-rabbit HRP-linked secondary antibodies in blocking buffer. Following wash, the blots were developed using the ECL-PLUS kit (Amersham) and the images captured on Hyperfilm-ECL.

Immunocytochemistry. Nodose ganglia were harvested as described above and processed in one of two ways. Fresh frozen nodose ganglia were cryosectioned (6–16 μm), collected on slides and postfixed with 3 % paraformaldehyde–lysine–periodate containing 0.1 % Triton X-100 for 5–10 min. This procedure gave the best results with the mAb Kv1.1. Alternatively, intact nodose ganglia were immersion fixed in 3 % paraformaldehyde overnight at 4 °C. They were cryoprotected with 5 % sucrose in isopentane for several hours, followed by 30 % sucrose. The tissue was frozen in liquid nitrogen and cryosectioned. All of the sections were blocked with PBS containing 3 % normal goat serum, 1 % bovine serum albumin for at least 30 min. If Triton X-100 was not used in the fixative, 0.3 % was added to the blocking solution. All primary antibodies were diluted 1 : 100. As a negative control, blocking solution followed by the appropriate secondary antibody was used. The fusion proteins were used to preabsorb the antibodies at a 1 : 1 μg concentration as a second negative control. After overnight incubation at 4 °C, the antibodies were visualized with either mouse or rabbit IgG tagged with fluorescein isothiocyanate or tetramethyl rhodamine isothiocyanate (TRITC), diluted 1 : 200 and incubated for 1.5 h at room temperature.

Electrophysiological methods

Electrophysiological experiments were performed on isolated neurons, 4–24 h after plating, using the whole-cell patch technique under voltage- or current-clamp conditions. Data were digitized and analysed using pCLAMP programs (Axon Instruments). Membrane potentials were not corrected for junction potentials that were measured to be 1–3 mV. Capacitance and series resistance were compensated unless otherwise noted. Electrodes (0.5–3.0 MΩ) were prepared from 7052 (Garner Glass Co.) or 8161 glass (WPI). The extracellular solution for perforated patch current-clamp recording contained (mM): 137 NaCl, 5.4 KCl, 1 $MgCl_2$, 2.0 $CaCl_2$, 10 glucose, 10 Hepes, pH adjusted to 7.3 with NaOH. The patch electrode (intracellular) solution contained (mM): 10 NaCl, 5 $MgCl_2$, 50 KCl, 50 K_2SO_4 and 10 Hepes, pH adjusted to 7.1 with KOH. The pipette solution included nystatin (25–50 μg ml^{-1}). For voltage-clamp experiments the bath solution contained (mM): 137 NaCl, 5.4 KCl, 1 $MgCl_2$, 2 $CaCl_2$, 10 glucose and 10 Hepes, pH adjusted to 7.3 with NaOH. K^+ currents were isolated by replacing Na^+ with *N*-methyl-D-glucamine (NMDG) and reducing Ca^{2+} to 0.02 mM. The pipette solution contained (mM): 145 K-aspartate, 5 NaCl, 1.95 $CaCl_2$, 2.2 EGTA, 2 $MgCl_2$, 10 glucose and 5 Hepes, pH adjusted to 7.2 with KOH. Tetrodotoxin (TTX, 10 μM) was added in some experiments to isolate the TTX-resistant sodium current in C-type neurons. Tetraethyl-ammonium (TEA), 4-aminopyridine (4-AP), α-dendrotoxin (α-DTX, CalBiochem) and Toxin K (Alomone) were used to characterize the K^+ currents in the whole-cell mode. All averaged data are shown as means ± S.E.M. unless otherwise noted. Statistical significance was determined at $P < 0.05$ using Student's *t* test.

Modelling methods

The voltage-clamp data for the α-DTX-sensitive K^+ current were used to formulate a Hodgkin-Huxley model of channel gating. The standard Hodgkin-Huxley two-state model of channel gating was used to describe the voltage dependence of steady-state activation ($\overline{dtx}$) and rate of activation (τ_{dtx}) according to:

$$\overline{dtx} = \frac{\alpha(V)}{\alpha(V) + \beta(V)}$$

and

$$\tau_{dtx} = \frac{1.0}{\alpha(V) + \beta(V)} + 10.0 \exp(-(0.07)^2(V+47)^2),$$

where

$$\alpha(V) = \frac{0.15(V+2.0)}{1.0 - \exp([V+2.0]/-7.0)}$$

and

$$\beta(V) = 0.0475 \exp\left(\frac{V+40.0}{-47.5}\right)$$

are the forward and reverse voltage-dependent rate constants, respectively. For all model simulations the equation for the DTX-sensitive current is:

$$I_{dtx}(V,t) = \overline{g}_{dtx}\, dtx(V - E_K),$$

where $\overline{g}_{dtx}$ corresponds to the maximum whole-cell conductance for the α-DTX-sensitive channels, and channel gating described

using a first-order time- and voltage-dependent differential:

$$\mathrm{d}dtx/\mathrm{d}t = (\overline{dtx} - dtx)/\tau_{\mathrm{dtx}}.$$

This current was incorporated into an existing model of nodose sensory neurons previously developed by our group (Schild *et al.* 1994). The whole-cell K^+ conductances used for modelling the voltage-clamp data were based upon model fits to the whole-cell K^+ current records using a non-linear parameter estimation routine. All subsequent simulations were performed using the original model formulations with adjustments to whole-cell capacitance and maximum whole-cell conductances in order to match the passive properties, action potential wave shape and discharge characteristics of each modelled cell. Simulations of the current-clamp recordings revealed the extent to which modulation of the α-DTX-sensitive current may impact resting membrane potential, threshold for discharge, action potential wave shape and repetitive discharge.

RESULTS

The identification of Kv1.1, Kv1.2 and Kv1.6 in nodose ganglia using RT-PCR

We determined that Kv1.1, Kv1.2 and Kv1.6 channel mRNA was present in nodose ganglia by RT-PCR using oligonucleotide primers specific to each channel (Fig. 1*A*). Since all three channels are expressed in rat brain, RT-PCR from rat brain poly-A RNA was used as a positive control. PCR products of the expected size (440, 577 and 50 bp for Kv1.1, Kv1.2 and Kv1.6, respectively) that hybridized to the internal oligonucleotide probes of either Kv1.1, 1.2 or 1.6 were detected in the PCR that included reverse transcriptase (+RT), but no signal was observed in the controls (−RT). We also examined the nodose ganglia for the presence of the β-subunits that may associate with the α-DTX-sensitive α-subunits. The Kvβ1.1, Kvβ1.3, Kvβ2 and Kvβ3 were present as PCR products (Fig. 1*C*). Northern blot analysis detected Kvβ1.2 in brain but not nodose ganglia (Fig. 1*B*).

To verify the expression of Kv channel protein in nodose ganglia as predicted by RT-PCR, we performed Western blots of tissue lysates for Kv1.1, Kv1.2 and Kv1.6. As seen in Fig. 2, anti-Kv1.1 detects a prominent band of ~70 kDa in brain as well as a similar sized band in nodose ganglia of comparable intensity that migrates slightly faster. Anti-Kv1.2 recognizes a band with a molecular weight greater than 75 kDa in brain lysate and nodose lysate. Anti-Kv1.6 detects a band of about 68 kDa in nodose lysate. We were not able to see Kv1.6 reactive bands in a comparable loading of rat brain lysate; however, we did detect bands when we examined the expression in 50 μg of a membrane-enriched fraction from rat brain. This suggests that Kv1.6 protein is more abundant in nodose ganglia relative to rat brain.

Expression of Kv1.1, Kv1.2 and Kv1.6 in nodose sensory neurons

Since the mRNA and proteins of Kv1.1, Kv1.2 and Kv1.6 were identified in nodose ganglia, we needed to verify their expression in the nodose neurons rather than non-neuronal cells of the ganglion. We used antibodies to the three K^+ channels to examine the distribution of the proteins in ganglia from both neonatal and adult rats. Kv1.1, Kv1.2 and Kv1.6 were present in all neurons of ganglia from neonatal animals and in a high percentage of neurons from the older animals. In three ganglia from the adult animal 89 % (1378/1542) of the neurons counted were positive for Kv1.1, 89 % (2541/2796) were positive for Kv1.2 and 97 % (1054/1086) were positive for Kv1.6. To examine the cellular distribution we dissociated the neurons to remove the closely apposed pericytes before the immunohistochemistry. Confocal sections through individual neonatal neurons showed that immunoreactivity against all three proteins had an intracellular distribution, probably in the endoplasmic reticulum, as well as appearing in patches at the surface membrane (arrows in Fig. 3*A*).

Fibres of sensory neurons of the nodose ganglion arise from several visceral regions. We were particularly interested in the neurons with afferent fibres in the aortic arch and upper respiratory tract because of our interest in properties of sensory activity initiated from these regions. Since not all adult neurons express Kv1.1, Kv1.2 and Kv1.6, we verified the expression of the proteins in these neurons by labelling the aortic depressor nerve and the superior laryngeal nerve. These neurons, identified by the presence of the tracer CM-DiI applied 5 days earlier, expressed Kv1.1, Kv1.2 and Kv1.6 as viewed with conventional fluorescent microscopy (Fig. 3*B*). In addition, Kv1.1 appeared especially prominent in the pericytes that surrounded the neurons. The section illustrating the co-localization with Kv1.2 also shows prominent distribution of Kv1.2 in the juxtaparanodal region as has been previously reported (Wang *et al.* 1993).

Expression of α-DTX-sensitive currents

α-DTX has a higher affinity for Kv1.1, Kv1.2 and Kv1.6 than for other voltage-gated potassium channels (Harvey, 1997). We used α-DTX as a tool to dissect the contribution of Kv1.1, Kv1.2 and Kv1.6 as a group to the total K^+ current. The total K^+ current in isolated neonatal neurons activated at potentials between −50 and −40 mV and increased with depolarization (Fig. 4*A*). In the presence of α-DTX (50 nM) the outward current was reduced at potentials more depolarized than −50 mV (Fig. 4*B*). The α-DTX-sensitive current, obtained by subtracting the current in the presence of α-DTX from that in its absence, was activated at approximately −40 to −45 mV and had the characteristics of a fast-activating K^+ current with very slow/no inactivation over 250 ms (Fig. 4*C*). α-DTX reversibly inhibited about 20 % (range 12–25 %) of the total K^+ current ($n = 9$) with near-maximum inhibition occurring at a concentration of 10 nM (Fig. 4*D*, compare 10 and 100 nM). Because of a few reports of higher EC_{50}

values for cloned expressed channels we also tested 500 nM *versus* 100 nM ($n = 2$) with no additional block. There were a few cells (8/107) that responded to α-DTX with a larger inhibition of 51 % of the total potassium current (range 45–61 %). These were not included in the averaged data.

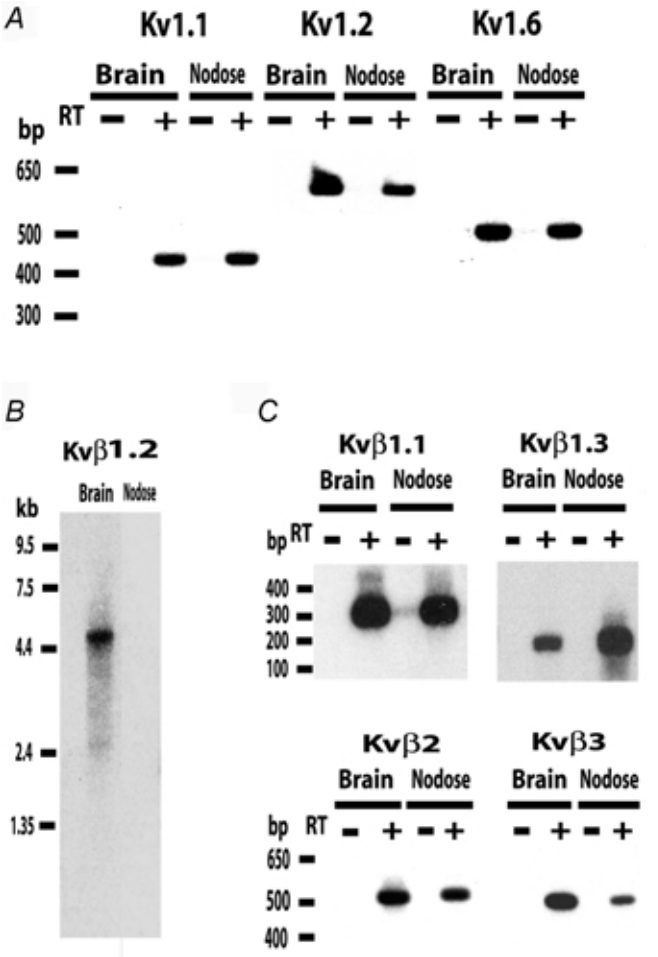

Figure 1. Expression of Kv1.1, Kv1.2, Kv1.6 and Kvβ subunit mRNA in rat nodose ganglia and brain

A, Kv1.1, Kv1.2 and Kv1.6 channel mRNAs are expressed in nodose ganglia. PCR products, resulting from the amplification of first-strand cDNA prepared with (+) or without (−) reverse transcriptase (RT) from nodose ganglia or brain poly A$^+$ RNA with Kv1.1, Kv1.2 or Kv1.6 specific oligomers, were separated by electrophoresis and transferred to nylon membranes. After Southern hybridization with ^{32}P-labelled specific internal oligomers (see Methods), the autoradiogram showed positive signals for all three channels from nodose and rat brain in the (+)-RT lanes with no signals in the control (−)-RT lanes. *B*, Northern blot analysis of Kvβ1.2 expression in adult rat nodose ganglia and brain. RNA size markers are indicated on the left. As shown, brain exhibited a single band of ~5 kb that hybridized with a Kvβ1.2 specific riboprobe, a band that is not present in nodose ganglia. *C*, RT-PCR analysis of the expression of Kvβ1.1, Kvβ1.3, Kvβ2 and Kvβ3 subunits in rat brain and nodose ganglia. As a control, first-strand cDNA reactions were performed either with (+) or without (−) RT. The oligonucleotide probes amplify a cDNA of 323 bp for Kvβ1.1, 182 bp for Kvβ1.3, 524 bp for Kvβ2 and 515 bp for Kvβ3.

Activation time for the α-DTX-sensitive current was obtained by best fit of the rising phase of the α-DTX-sensitive current to a single exponential function. The activation τ was voltage dependent, 6.5 ± 1.0 ms at 0 mV and 17 ± 3.2 ms at −20 mV ($n = 5$, Fig. 5*A*). The voltage dependence of activation was obtained from the tail current amplitudes at −100 mV following steps of −70 to +20 mV. Half-maximal activation, as determined by a Boltzman fit, was −17.6 mV with a slope factor of 8.7 ($n = 5$, Fig. 5*B*). The voltage dependence of activation was obtained from the tail current amplitudes at −100 mV following steps of −70 to +20 mV. Deactivation, obtained from single exponential fit to the tail current at −100 mV following a step from 20 mV, occurred with $\tau = 4.6 \pm 1.6$ ms, $n = 6$). It is important to note that kinetic values for the α-DTX-sensitive current recorded in cells in which the perforated patch was used did not differ from those obtained with the open patch. The model-generated activation characteristics (described below) are shown superimposed on the experimental data in Fig. 5.

Sensitivity to 4-AP and TEA

Kv1.1, Kv1.2 and Kv1.6, heterologously expressed, are sensitive to low concentrations of 4-aminopyridine ($IC_{50} \leqslant 1$ mM, Stuhmer *et al.* 1989; Klumpp *et al.* 1991; Grissmer *et al.* 1994). Therefore, 5 mM 4-AP would be expected to block all α-DTX-sensitive current. Neurons were first exposed to α-DTX to verify inhibition of the current that was reversed fully upon washout of the α-DTX. Then 4-AP (5 mM) was applied to the neurons followed by α-DTX in the continued presence of 4-AP. There was no further decrease in current upon the addition of α-DTX ($n = 5$, Fig. 6*A*). Thus the α-DTX-sensitive current in nodose neurons is a subcomponent of the 4-AP-sensitive current. The remainder of the 4-AP-

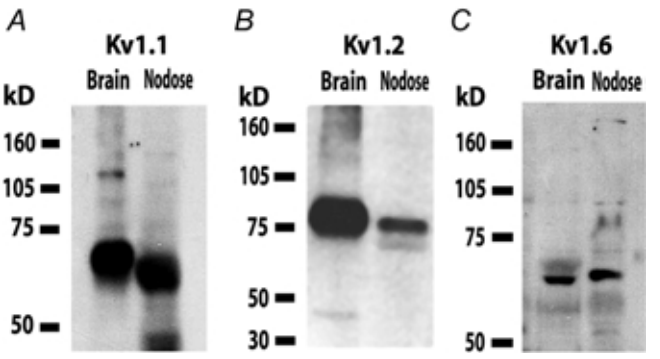

Figure 2. Kv1.1, Kv1.2 and Kv1.6 are detected in Western blots of nodose ganglia and brain protein

Western blots of channel expression in nodose ganglia (*A, B* and *C*), brain lysates (*A* and *B*) and brain crude membrane fraction (*C*) probed with monoclonal anti-Kv1.1 (*A*), monoclonal anti-Kv1.2 (*B*) and polyclonal anti-Kv1.6 (*C*) (50 μg protein per lane). Immunoreactive bands were visualized with ECL-Plus (Amersham Pharmacia Biotech). Molecular weight markers (kDa) are indicated on the left.

sensitive current that was not affected by DTX had at least two kinetically different components, transient and slowly decaying. These have not yet been explored, although our preliminary immunohistochemical data suggest the presence of at least two or more additional 4-AP-sensitive channels.

In contrast to the 4-AP sensitivity, homomultimers of heterologously expressed Kv1.1, Kv1.2 and Kv1.6 are markedly different in sensitivity to TEA. The IC_{50} values for TEA block of Kv1.1 and Kv 1.6 are low, $\leqslant 1$ mM and ~2–7 mM, respectively, while the IC_{50} for Kv1.2 is reported to be over 100 mM (Stuhmer *et al.* 1989; Christie *et al.* 1990; Grupe *et al.* 1990; Kirsch *et al.* 1991; Klumpp *et al.* 1991; Grissmer *et al.* 1994; Gomez-Hernandez *et al.* 1997). In the next set of experiments the K^+ currents were examined in the presence of 5 mM TEA, a concentration expected to block both Kv1.1 and Kv1.6 but to have no effect on Kv1.2. There was no further effect of addition of α-DTX in the presence of 5 mM TEA ($n = 4$, Fig. 6*B*). This suggests that Kv1.2 does not form a homomultimer but associates as a heteromultimer with Kv1.1 and/or Kv1.6 to form a channel whose sensitivity to TEA is similar to the latter two subunits (D'Adamo *et al.* 1999). An alternative explanation is that homomultimers of Kv1.2 exist in low density. A maximal concentration of Toxin K (10 nM), a

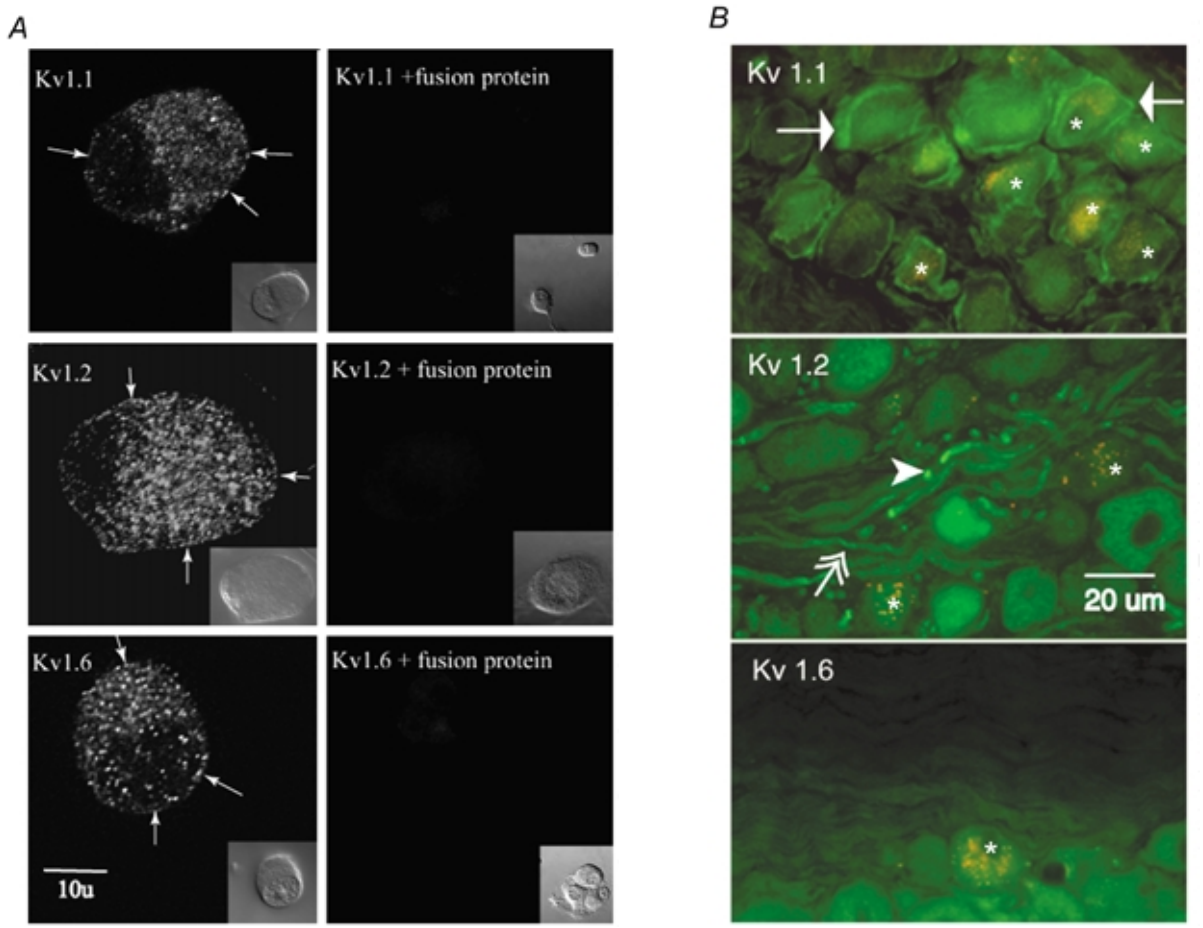

Figure 3. The localization of Kv1.1, Kv1.2 and Kv1.6 immunoreactivity

A, left panels show confocal single slice images through isolated neonatal nodose neurons labelled with Kv1.1 (top), Kv1.2 (middle) and Kv1.6 (bottom). The arrows indicate some regions where patches of immunoreactivity appear at the cell membrane. Differential interference contrast (DIC) images of the cells appear in insets in each panel. Right panels show preabsorption controls with the immunizing fusion protein for the three antibodies. *B*, expression of Kv1.1, Kv1.2 and Kv1.6 in superior laryngeal sensory neurons is shown with conventional fluorescent microscopy of 6 μm sections through the nodose ganglion. The Cm-DiI label was co-localized with the potassium channel antibodies (green) to give a yellow–orange colour. These images were digitally recorded as single labels and then superimposed. These figures also illustrate a wide distribution in the level of immunoreactivity among the neurons. The arrows in the upper panel show that Kv1.1 immunoreactivity is also found in pericytes surrounding the neurons. The section in the middle panel contains a group of nerve fibres. The arrowhead indicates Kv1.2 immunoreactivity in the juxta-paranodal regions of a myelinated fibre and the double-headed arrow indicates immunoreactivity distributed along a finer fibre. In all panels the asterisks identify neurons containing DiI.

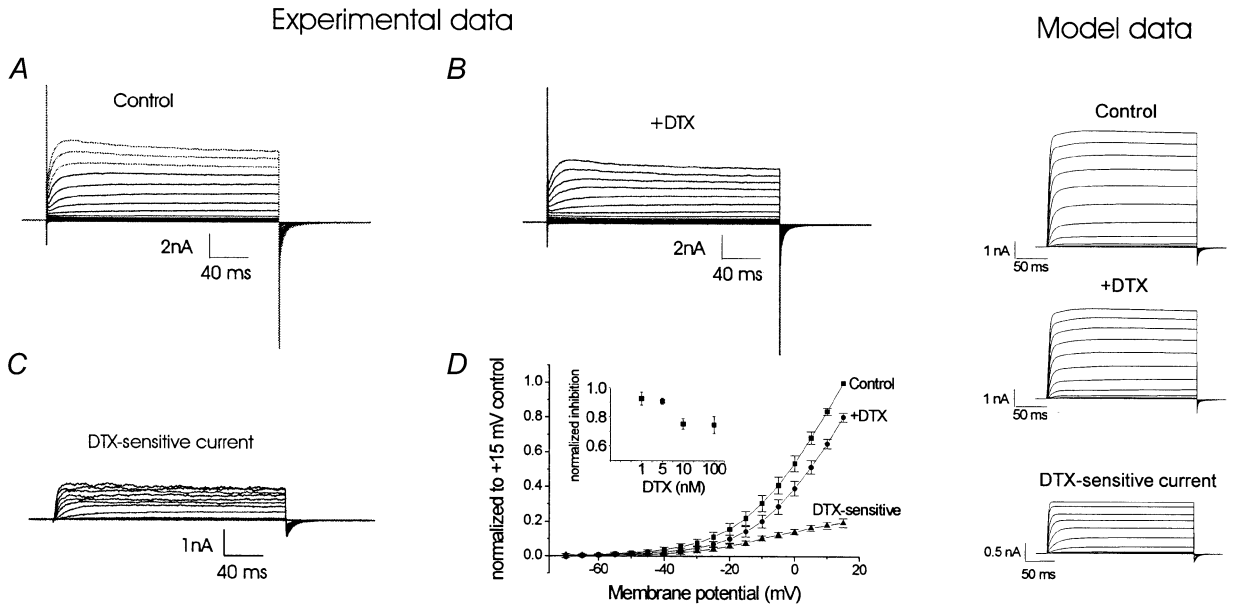

Figure 4. Effect of α-DTX on potassium currents

In the left panel experimental data illustrate an example of current in a baroreceptor C-type neuron elicited by a series of 250 ms polarizing pulses from to −100 to +30 mV in 10 mV steps from a holding potential of −80 mV in the absence (*A*) and presence (*B*) of 50 nm α-DTX. The α-DTX-sensitive current (*C*) was obtained by subtracting *B* from *A*. *D* shows the composite of current–voltage relationships of α-DTX-sensitive current of 8 neurons where voltage steps were delivered in 5 mV steps. The inset illustrates the concentration–response relationship for 5 neurons. Capacitance was not compensated in the experiment shown in *A*. The right panel illustrates the model-derived whole-cell K^+ current data matched to the experimental data presented on the left. Maximum whole-cell K^+ conductances were as follows (all in nS): $g_{dtx} = 7.5$, $g_{4\text{-}AP} = 37.5$, $g_{K,Ca} = 7.5$ and $g_K = 17.5$.

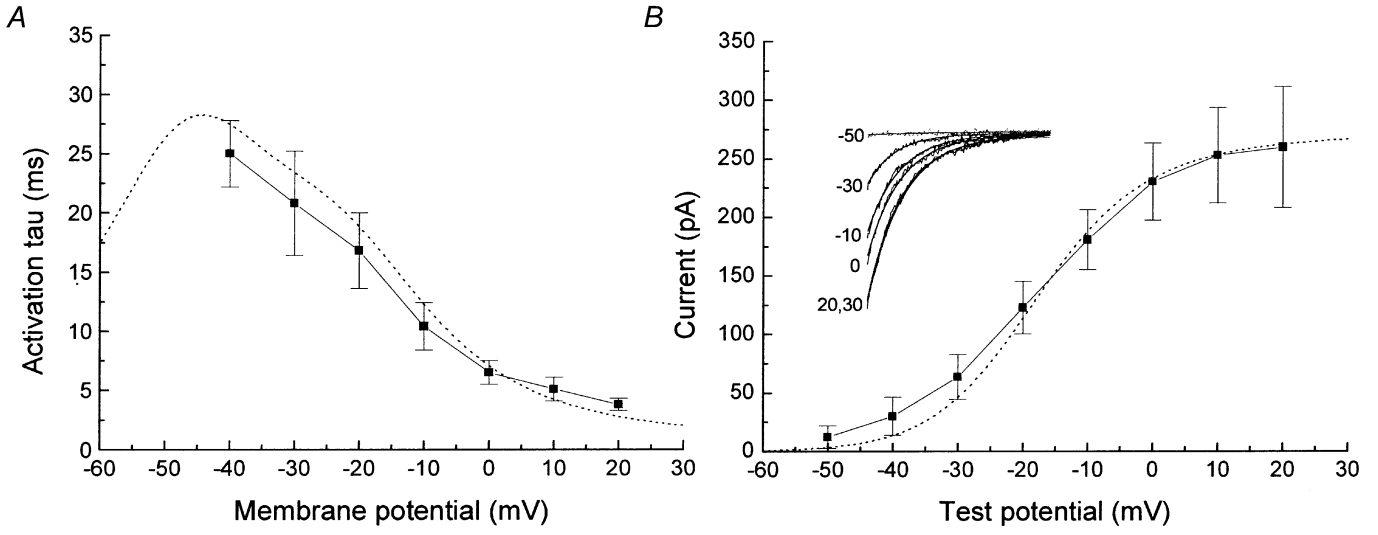

Figure 5. Characteristics of activation

A, the voltage dependence of the activation times was obtained by a single exponential fit to the rising phase of the α-DTX-sensitive current at each potential. *B*, voltage dependence of activation was obtained from tail current measurements at −100 mV following 10 mV depolarizing steps to −70 to +20 mV from a holding potential of −90 mV. The model simulation of the data is indicated by the dotted lines in *A* and *B*. A non-linear parameter estimation technique was used to identify forward and reverse voltage-dependent rate constants that produced the best least-squares fit to the α-DTX-sensitive K^+ current data.

toxin that is highly selective for Kv1.1 (Robertson *et al.* 1996) blocked only 62 % (range 47–72 %, $n = 4$) of the α-DTX-sensitive current at +20 mV, which indicates that Kv1.1 is not solely responsible for the α-DTX-sensitive current in the somal membrane.

A- *versus* C-type neurons

The vagus nerve, which carries the nerve fibres of the nodose ganglion, contains 10–15 % myelinated axons of A-type neurons and 85–90 % unmyelinated axons of C-type neurons (Evans & Murray, 1954; Agostoni *et al.* 1957; Hoffman & Kuntz, 1957). The two types have quite different properties when studied *in situ*. In general, A-type sensory receptors are low-threshold, rapidly conducting mechanoreceptors while C-type receptors are slow-conducting high-threshold mechanoreceptors or chemoreceptors. Previous studies of nodose ganglia from adult rats demonstrated that the α-DTX-sensitive current was present in A-type neurons (Stansfeld *et al.* 1986). This raised the possibility of a selective distribution of the channels. However, our immunocytochemical and electrophysiological studies supported the functional presence of the α-DTX-sensitive channels in all neonatal neurons, both A- and C-type cells. However, since not all adult neurons express these Kv1 family members as demonstrated by the immunocytochemistry, we explored the effects of α-DTX on neurons from older animals (postnatal days 21–60). Fourteen per cent (22/155) of neurons from the older animals did not respond to α-DTX. In a subset of these experiments, we segregated C- from A-type neurons by examining each neuron for the presence of TTX-resistant sodium current in physiological saline before application of α-DTX in the K^+ current-isolating solution. Those for which the sodium current was completely blocked by TTX were categorized as A-type. Those that also had TTX-resistant sodium current were designated as C-type, although it is possible that a small portion of the A-type neurons conducting in the near C-type range have some TTX-resistant current (Stansfeld & Wallis, 1985). In these studies the α-DTX-sensitive current was present in 33/39 C-type neurons and 13/15 A-type neurons and represented approximately 20 % of the total outward K^+ current at the end of a voltage step to +20 mV. There were no obvious differences in the voltage- and time-dependent characteristics of the α-DTX-sensitive current between these two functionally distinct populations of sensory neurons. Thus, both A- and C-type neurons expressed α-DTX-sensitive current similarly.

Model formulation and testing

The K^+ current recordings and averaged data presented above were used to develop a Hodgkin-Huxley two-state model of channel gating for the α-DTX-sensitive current (I_{dtx}). Acceptable fits to any particular data set required subtle

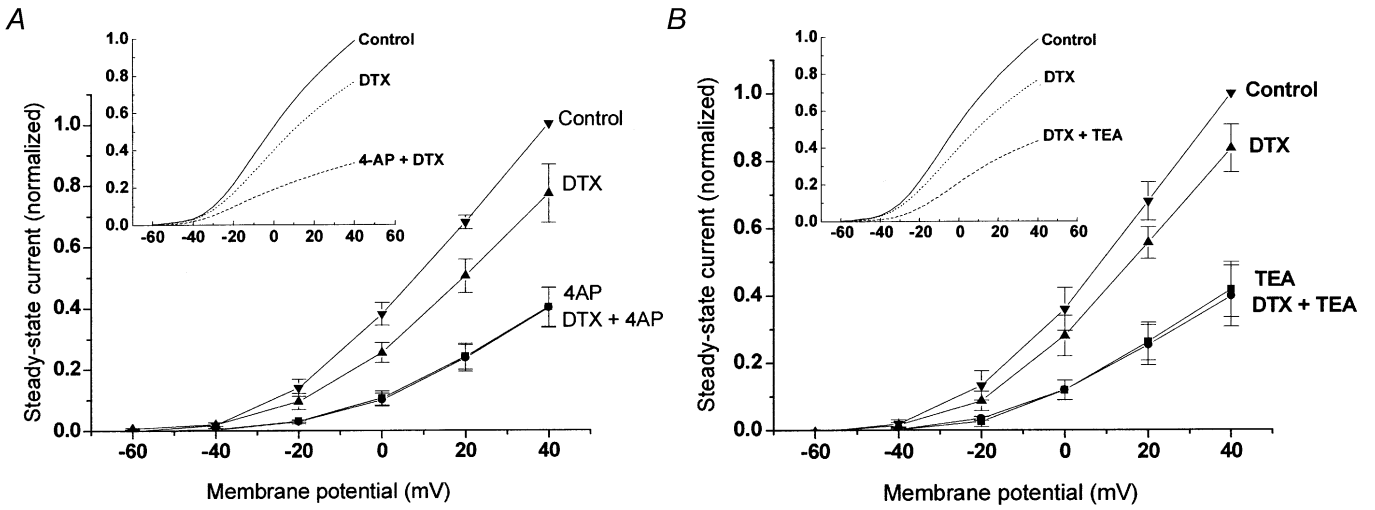

Figure 6. Sensitivity to 4-AP and TEA

A, α-DTX-sensitive current is a subcomponent of the 4-AP-sensitive current. The current–voltage relationship was obtained at the end of the voltage pulse, as in Fig. 4 in control conditions (▼), after addition of 50 nM α-DTX (▲), followed by 5 mM 4-AP after washing the DTX (■) and subsequent addition of α-DTX to the 4-AP perfusion (●). Addition of α-DTX in presence of 4-AP produced no further inhibition of the current. *B*, the α-DTX-sensitive current is a subcomponent of the TEA-sensitive current. Addition of α-DTX in the presence of 5 mM TEA (●) produced no further inhibition from that seen in the presence of 5 mM TEA alone (■), although the cells were shown to be sensitive to α-DTX (▲). The insets in *A* and *B* give the model-derived current–voltage relationships for the total K^+ current and the total K^+ current minus the α-DTX-sensitive component (DTX) and either both the α-DTX- and 4-AP-sensitive currents (4-AP + DTX in *A*) or both the α-DTX- and TEA-sensitive currents (DTX + TEA in *B*). Model parameters and maximum whole-cell K^+ conductances were the same as those for the model data of Fig. 4.

parameter adjustments related to the voltage-dependent channel gating equations, generally representing less than a 10% change in any particular model parameter (e.g. half-activation potentials, slope of the activation function). These equations were then incorporated into the existing ionic current model of nodose sensory neurons (Schild *et al.* 1994; Schild & Kunze, 1997). The model was initially modified to account for the solutions and test protocols used to collect the whole-cell K^+ current data. Using subtracted records along with the total whole-cell K^+ current a parameter estimation routine was used to determine the relative contribution of the TEA-sensitive (I_K), 4-AP-sensitive ($I_{4\text{-}AP}$), Ca^{2+}-activated ($I_{K,Ca}$) and α-DTX-sensitive K^+ currents to the total outward K^+ current (Fig. 6 insets). For the pooled voltage-dependent steady-state data only the maximum whole-cell conductances of the individual K^+ currents were adjusted. All other modelling parameters remained constant.

Functional role of α-DTX-sensitive current at the soma

In order to explore the functional impact of I_{dtx} on resting membrane potential, activation threshold, action potential wave shape and repetitive discharge, whole-cell membrane potential recordings were obtained in current-clamp mode using the perforated patch technique. For analysis of these data, the model was returned to a configuration consistent with the current-clamp recording protocols. Unless otherwise noted, all parameters for the I_{dtx} gating variable and the relative whole-cell conductances for the model K^+ currents were the same as those used to match the pooled steady-state data (Figs 5 and 6). The experimental data did not reveal differences in α-DTX-sensitive current dynamics between A- and C-type neurons, so both were simulated using an identical parameter set for I_{dtx}.

Resting potential. Under current clamp, the neurons maintained a stable resting potential of −58.6 ± 1.5 mV (range −44.5 to −77 mV, $n = 28$) in normal physiological solution. Application of α-DTX (50 nM) produced no consistent change in resting membrane potential, even when depolarized (via current injection) to voltages as low as −45 mV (Fig. 7). Above −45 mV, application of α-DTX depolarized the cells, consistent with its activation range. The extent of depolarization increased as the membrane voltage was pushed further into the activation region for I_{dtx}. The effect of the magnitude of I_{dtx} upon the resting membrane potential was investigated using the model by varying its maximum whole-cell conductance. Over the range of whole-cell conductances (7.5–15.0 nS) required to match the voltage-clamp data there was little impact in the range of the normal resting membrane potential in the A- and C-type neuron models (Fig. 7, lines). Only a shift in the voltage-dependent activation function toward more negative potentials or a dramatic increase in the slope of the steady-state activation curve (Fig. 5*B*) could effect a larger change in membrane potential when the α-DTX current was removed. However, such changes would be inconsistent with the fits to the observed experimental data (Figs 5 and 6).

Action potential. The action potential elicited in A-type neurons in response to a depolarizing stimulus in the presence of α-DTX showed only a small increase in amplitude (0.6 ± 0.7 mV, range 0–1.4 mV, $n = 6$) and in duration (0.3 ± 0.22 ms, range 0–0.6 ms, $n = 6$), neither of which was significant ($P > 0.1$; Fig. 8*A*). C-type neurons also responded with a small but more variable increase in amplitude (1.9 ± 2.8 mV, range 0–9 mV, $n = 6$, $P > 0.1$) and duration (1.1 ± 0.7 ms, range 0–2.0 ms, $n = 6$, $P > 0.1$, Fig. 8*B*). Larger effects tended to occur in cells with the broader control action potentials with stronger TTX-resistant sodium currents but within the C-type group the data were not significantly different from control values. However, the peak of the after-hyperpolarization (AHP) was decreased significantly in the presence of α-DTX for A-type (−2.9 ± 1.7 mV, range −0.7 to −6.3 mV; $n = 6$) and to a slightly greater extent for C-type neurons (−3.3 ± 2.3 mV, range −1.0 to −9.0 mV, $n = 7$, $P < 0.01$ for both A- and C-types).

The role of I_{dtx} in shaping neuronal action potentials was studied using the A- and C-type models. Background currents were adjusted so that both models exhibited resting membrane potentials close to −60 mV to ensure comparable initial conditions for I_{dtx} in both models. Typically, the model required a lower current magnitude than the experimental recordings to achieve discharge threshold. Less current was required because the model did not account for current leakage around the patch electrode,

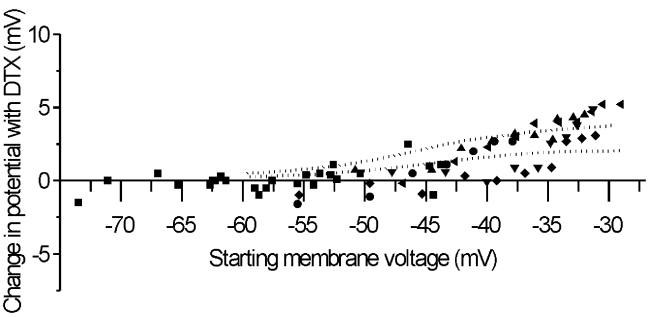

Figure 7. Effects of α-DTX on membrane potential

α-DTX has no effect on membrane potential in the resting range but depolarizes the neurons if applied at potentials more positive than −50 mV. The change from the resting potential upon application of α-DTX (50 nM) is plotted against the resting membrane potential, $n = 28$ (■). The effects of α-DTX for 5 neurons (▼, ▲, ●, ◆ and ◀) held (via current injection) at more depolarized potentials are also shown. The lines demarcate the change in the resting potential upon removal of the α-DTX-sensitive current (I_{dtx}) as demonstrated by the model. The upper line corresponds to a maximum whole-cell conductance of 15 nS for I_{dtx}, while the lower corresponds to 7.5 nS.

the extent of which was different for each recording. However, the relative range of current magnitudes required by the model followed reasonably well the range of current magnitudes required to evoke repetitive discharge in the recorded cells (e.g. multiples of threshold stimulus magnitude produce comparable responses).

As in our experimental data, four consistent changes in action potential wave shape were apparent in both cell types, albeit to a much lesser extent in the A-type (Fig. 8*C*) than the C-type neurons (Fig. 8*D*). The threshold for discharge decreased, the peak amplitude and the duration of the action potentials were greater and the depth of the after-hyperpolarization was consistently less with I_{dtx} removed. These observations suggest that the measured changes in action potential peak and duration, while not statistically significant, may in fact be real. The practical aspects associated with patch recording of membrane properties (e.g. fluctuations in resting membrane potential of a few millivolts, recording noise, small changes in seal and access resistances) make difficult the comparison of subtle changes in discharge threshold and action potential wave shape. The model simulations enabled precise manipulation of membrane conductances so that comparisons between control and test data could be performed in the knowledge that all other conditions were identical. Since the model of I_{dtx} was based upon voltage-clamp data from nodose neurons and simulations were in good agreement with the global effects of α-DTX upon action potential discharge, the subtle, experimentally observed changes in action potential wave shape may indeed reflect an underlying role for I_{dtx}.

Repetitive activity. A series of depolarizing current steps of increasing amplitude was applied from the resting potential. Across the population of C-type neurons, responses to depolarizing current injection (0–400 pA) ranged from single action potentials to short bursts of action potentials or sustained discharge. An illustration of a less excitable C-type cell and its model companion is presented in Fig. 9*A*. The most consistent observations in all current-clamp recordings and model simulations were that α-DTX reduced the depolarizing current needed to elicit an action potential(s) and that the cells tended to be

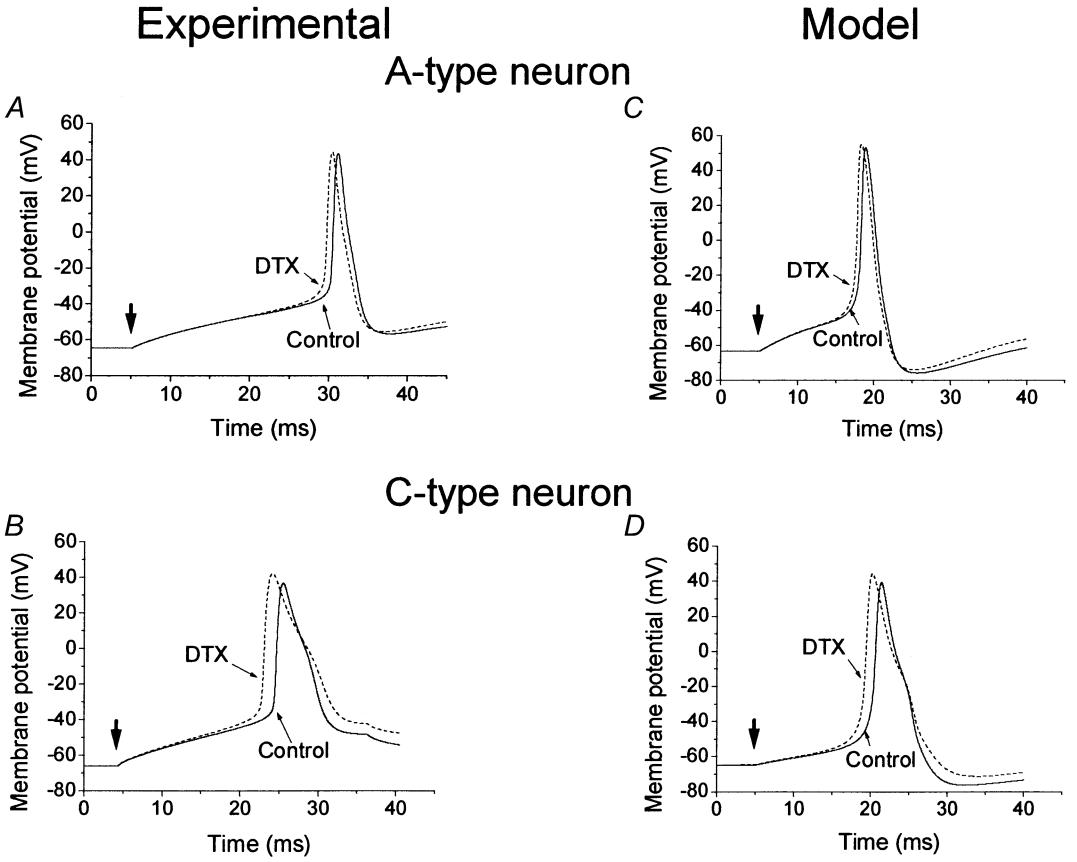

Figure 8. Effect of α-DTX on the action potentials of A- and C-type neurons

The left panels show experimental data for an A-type neuron (*A*) depolarized from −65 mV using a 60 pA step current and a C-type neuron (*B*) depolarized from −66 mV with a 50 pA step current. The right panels present simulation data for an A-type model neuron using a 50 pA step current (*C*) and a C-type model neuron using a 20 pA step current (*D*). For all traces, the dotted lines present the neuron responses to the same step current magnitudes as in control conditions but in the presence of α-DTX. Arrows indicate the start of the current injection.

more excitable at lower stimulus intensities. Such elevation in excitability, manifest as an increase in frequency of discharge and/or number of action potentials in a burst at the same depolarizing stimulus, was apparent in all but one C-type cell recording (18/19). The exception responded with the typical decrease in threshold but with no elevation in the number of action potentials produced over its burst response. Examples are given in Fig. 9*B* of five C-type neurons responding to a depolarizing current injection in the presence and absence of α-DTX. Three of the five (upper panel) had only a single action potential in response to depolarization before addition of α-DTX.

Across the population of A-type neurons studied, current steps tended to elicit repetitive discharge patterns far less variable than C-type cells. In both the experimental recordings ($n = 6$) and model studies, A-type neurons responded to the loss of the α-DTX-sensitive current in a manner similar to that exhibited by C-type cells with a reduction in the threshold stimulus needed to elicit an action potential(s). Although A-type neurons tended to become more excitable at lower stimulus intensities, the overall effect of removal of α-DTX-sensitive current was far less pronounced than was observed for C-type cells. At all stimulus intensities that elicited repetitive discharge,

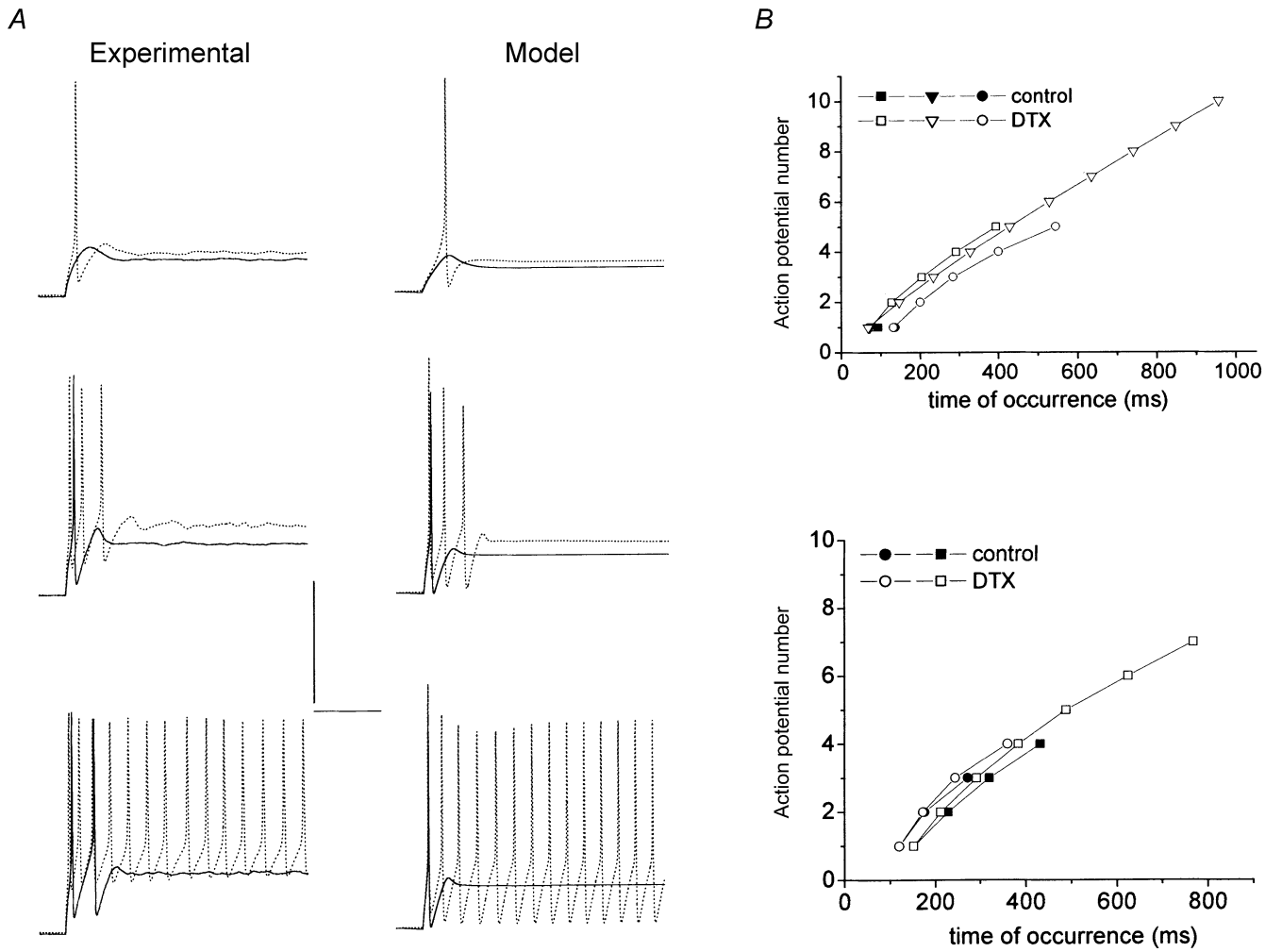

Figure 9. α-DTX increases excitability in C-type neurons

A, on the left is shown the discharge of a C-type neuron in response to 80, 200 and 280 pA current steps from a resting membrane potential of approximately −70 mV under control conditions (continuous line) and in the presence of α-DTX (dotted line). On the right is shown a C-type model neuron configured to match the resting membrane potential and action potential discharge properties of the control cell. Simulation results present discharge in response to 15, 60 and 100 pA current steps under control conditions (continuous line) and with g_{dtx} equal to zero to simulate the application of α-DTX (dotted line). Maximum whole-cell K^+ conductances were as follows (all in nS): $g_{dtx} = 12.5$, $g_{4\text{-}AP} = 30$, $g_{K,Ca} = 30$ and $g_K = 15$. For all traces the horizontal and vertical scale bars correspond to 250 ms and 60 mV, respectively. *B*, occurrence of action potentials in response to a step depolarizing current in control solution (closed symbols) and in the presence of α-DTX (open symbols) for 3 C-type neurons (upper panel) that fired only a single action potential before addition of α-DTX and two neurons (lower panel) that fired with a burst before α-DTX.

the firing rate of A-type neurons showed only a modest increase in the presence of α-DTX (Fig. 10).

Model predictions of K^+ current dynamics

Over the course of an action potential the four major currents responsible for repolarization are the delayed rectifier (I_K), calcium-activated potassium current ($I_{K,Ca}$), the 4-AP-sensitive current with transient and slowly decaying components ($I_{4\text{-}AP}$) and I_{dtx}, as described in the present report.

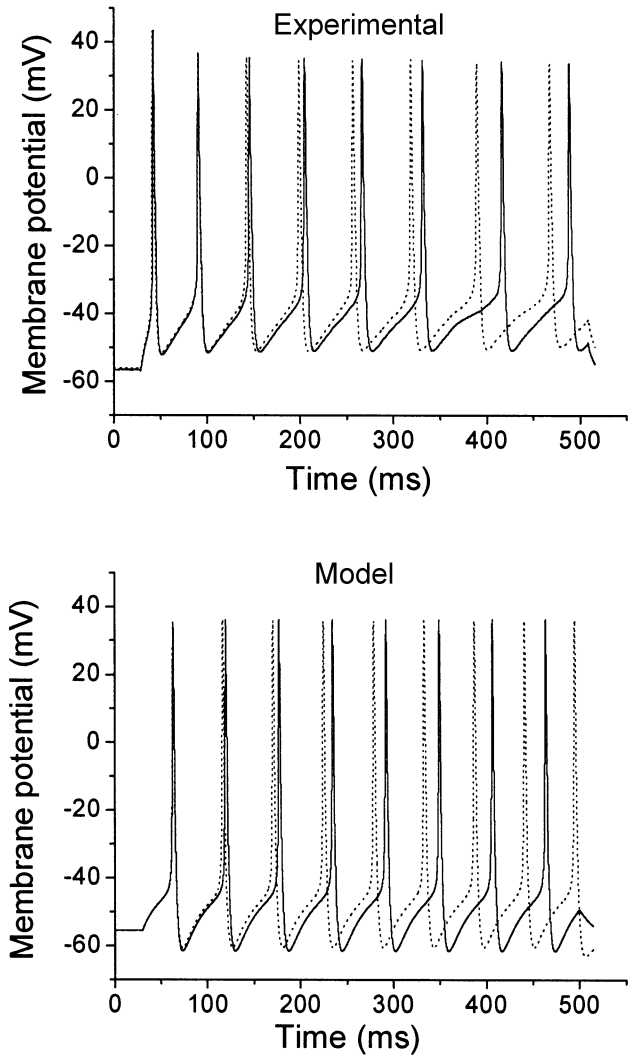

Figure 10. α-DTX increases firing frequency in A-type neuron

Top panel, discharge of an A-type neuron in response to a 100 pA current step from a resting membrane potential of −58 mV under control conditions (continuous line) and in the presence of α-DTX (dotted line). Bottom panel, A-type model neuron configured to match the resting membrane potential and action potential discharge properties of the control cell. Simulation results present discharge in response to a 70 pA current step under control conditions (continuous line) and with g_{dtx} equal to zero to simulate the application of α-DTX (dotted line). Maximum whole-cell K^+ conductances were as follows (all in nS): $g_{dtx} = 7.5$, $g_{4\text{-}AP} = 40$, $g_{K,Ca} = 2.0$ and $g_K = 12.5$.

The C-type model revealed that I_{dtx} was one of the largest outward currents at peak membrane voltages even though I_{dtx} represented only 20–25 % of the total steady-state outward K^+ current (Fig. 11*C*). This was due to the rapid rate of activation for I_{dtx} at depolarized potentials as well as a general lack of inactivation (Figs 4 and 5). Near the peak of the control action potential $I_{K,Ca}$ and $I_{4\text{-}AP}$ were about the same magnitude but ~35 % smaller than I_{dtx}. Both $I_{K,Ca}$ and $I_{4\text{-}AP}$ increased in response to the removal of I_{dtx}, although by different amounts and with different time course. The combination of the modest upstroke velocity of C-type neurons (as compared to A-type), the broader action potential waveform, the transient (inactivating) component of the 4-AP-sensitive current and a prominent inward Ca^{2+} current resulted in a slightly greater recruitment of $I_{K,Ca}$ than $I_{4\text{-}AP}$ (Fig. 11*C* and *D*). The net increase in these two currents and the modest increase in I_K were not sufficient to entirely offset the loss of I_{dtx}. Thus, during the upstroke of the action potential the membrane voltage achieved a greater peak height. But even this additional depolarization could not recruit a comparable total outward K^+ current and, as a result, repolarization was delayed and the C-type action potentials tended to broaden (Fig. 8*D*). Both $I_{K,Ca}$ and $I_{4\text{-}AP}$ decayed rapidly upon the initial phase of repolarization but $I_{K,Ca}$ slowed considerably over the start of the AHP, when it functioned to limit the recovery of membrane voltage, although not as effectively as with I_{dtx} present, so the AHP was less pronounced (Fig. 8*D*).

A-type neurons were modelled using identical formulations for I_{dtx} to those in the C-type neuron model. Both models produced about the same peak magnitude of this current (Fig. 11*A* and *C*). However, the total outward K^+ current in A-type cells has a large 4-AP-sensitive component (Schild *et al.* 1994). The magnitude and time course of $I_{4\text{-}AP}$ was comparable to that of I_{dtx}. Together, $I_{K,Ca}$ and I_K provided less than 30 % of the total repolarization current over the rapid phases of discharge but both of these currents contributed significantly over the time course of the AHP. The rapid upstroke velocity and short duration of A-type action potentials appealed to the rapid dynamics of the transient component of $I_{4\text{-}AP}$. With the removal of I_{dtx}, $I_{4\text{-}AP}$ was able to compensate with a large and fast repolarizing current. As a result, there was very little change in peak height or duration of the A-type action potential (Fig. 8*A* and *C*). An additional factor that facilitated repolarization is that A-type neurons lack the slow TTX-resistant Na^+ current that limits the effectiveness of the total outward K^+ current and thereby delays repolarization (Schild *et al.* 1994; Schild & Kunze, 1997). The combination of a rapid upstroke and a naturally brief action potential duration meant that the increased $I_{4\text{-}AP}$ was a more effective repolarizing current and, as a result, the overall impact of removing I_{dtx} upon an A-type action potential was more modest than in C-type neurons (Fig. 8*D*).

DISCUSSION

Expression of Kv1.1, Kv1.2 and Kv1.6 in nodose neurons

These studies are the first to demonstrate the presence of Kv1.1, Kv1.2 and Kv1.6 in visceral sensory neurons and to demonstrate the functional role of their α-DTX-sensitive current. They also extend previous findings (Stansfeld *et al.* 1986) to show that not just A-type, but also the larger population of C-type neurons express α-DTX-sensitive current. Since these Kv1 family members, studied in heterologous expression systems, are quite similar with regard to their electrical properties, we treated them as a single α-DTX-sensitive current for a functional assessment of their contribution to the activity of these neurons. The kinetic and voltage-dependent features of the α-DTX-sensitive current are comparable to those reported whether expressed as homomeric channels or together as heteromeric channels (Christie *et al.* 1989; Stuhmer *et al.* 1989; Grupe *et al.* 1990; Kirsch *et al.* 1991; Bertoli *et al.* 1994; Moran & Conti, 1995; Sprunger *et al.* 1996; D'Adamo *et al.* 1999). Activation τ values reported for Kv1.1, Kv1.2 and Kv1.6, as either τ or $\tau_{½}$, fall within the range of 2–12 ms at 0 mV (Christie *et al.* 1989; Kirsch *et al.* 1991; Bertoli *et al.* 1994; Wang *et al.* 1998). This correlates well with our value of 6.5 ± 1.0 ms at 0 mV. The $V_{½}$ for the DTX-sensitive current in our studies occurred at −17 mV. By comparison, there is a broad range, from −6 to −37 mV, for previously reported values of $V_{½}$ for these three channels expressed individually. However, where the same laboratory has compared Kv1.1 and Kv1.2, most of the activation curves for Kv1.2 fall to the right of those of Kv1.1 by at least 10 mV (Stuhmer *et al.* 1989; Christie *et al.* 1990; Grissmer *et al.* 1994; Hopkins *et al.* 1994; D'Adamo *et al.* 1999). Kv1.6 has been less frequently studied and its range has been reported as −12 to −30 mV (Grupe *et al.* 1990; Kirsch *et al.* 1991; Bertoli *et al.* 1994). Slope factors for all three channels fall within the range of 6–13 mV (Stuhmer *et al.* 1989; Christie *et al.* 1990; Grupe *et al.* 1990; Kirsch *et al.* 1991; Klumpp *et al.* 1991; Bertoli *et al.* 1994; Grissmer *et al.* 1994; Moran & Conti, 1995; Hopkins, 1998; D'Adamo *et*

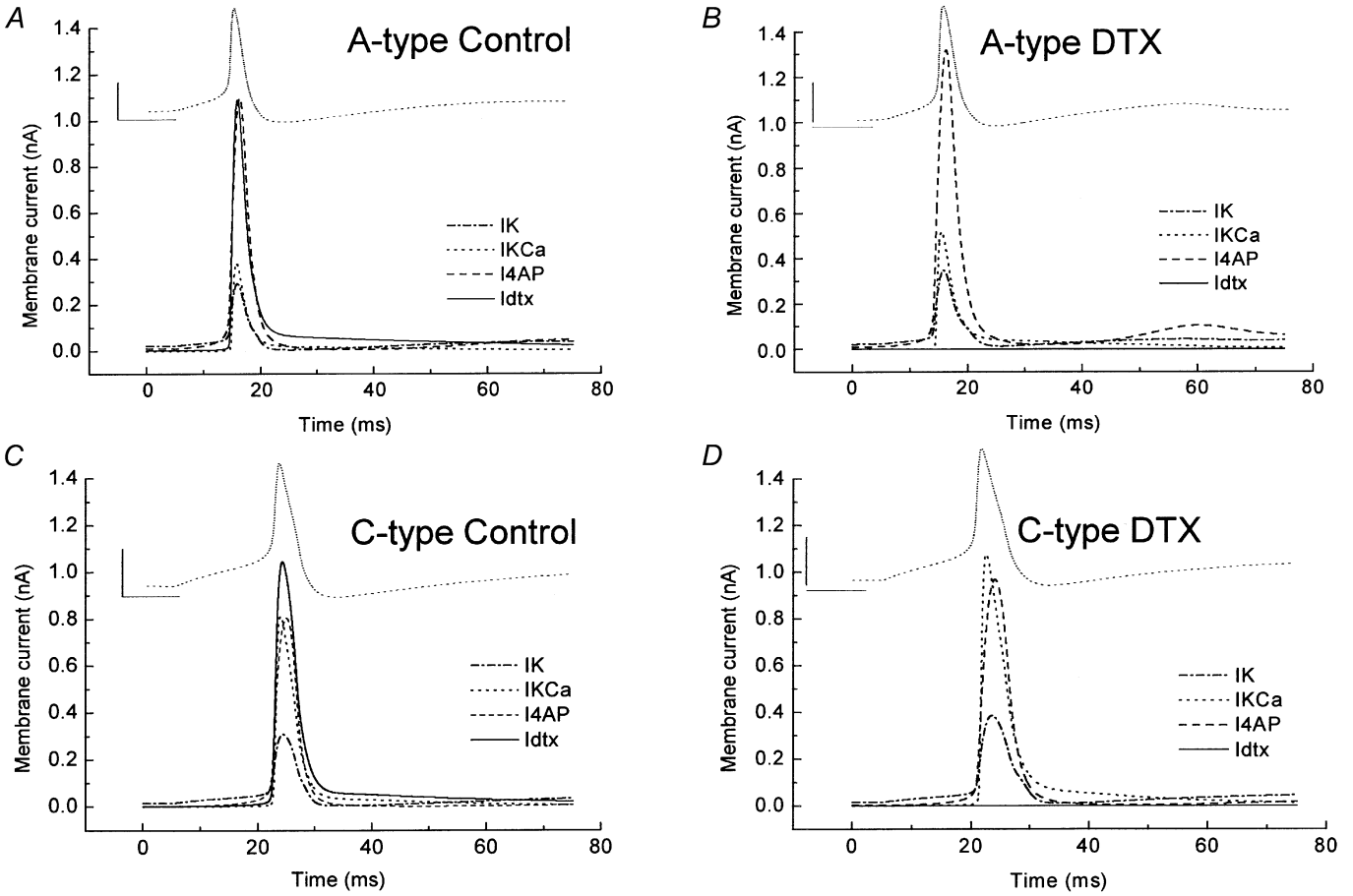

Figure 11. Time course of outward K+ currents in model A- and C-type neurons

The 4 major K+ current components from A-type (*A* and *B*) and C-type model neurons (*C* and *D*) under control conditions (*A* and *C*) and after the removal of I_{dtx} (*B* and *D*). The C-type and A-type models utilized the same values of parameters for the model data presented in Figs 9 and 10, respectively. Corresponding A-type and C-type action potentials evoked using a 60 and 40 pA, respectively, step current injection are shown above for reference. Action potential calibration bars, 10 ms, 40 mV.

al. 1999). Kv1.1 co-expressed with Kv1.2 has a reported $V_{½}$ of −16 to −33 mV with slope factors of 5.9–11 mV (Christie *et al.* 1990; Hopkins *et al.* 1994; Hopkins, 1998; D'Adamo *et al.* 1999). Our deactivation τ of 4.6 ms at −100 mV matches comparable data in the literature of about 5 ms at −80 mV for both Kv1.1 and Kv1.2. (D'Adamo *et al.* 1999) and 5 ms for Kv1.2 at −100 mV (Sprunger *et al.* 1996). The presence of mRNA for several Kvβ subunits indicates that these proteins may play a role in determining kinetics and density of the expressed α-DTX-sensitive channels in nodose ganglia.

While the pharmacology and immunocytochemical experiments support the presence of the proteins in the soma, we do not have data to argue for specific subunit combinations in the nodose neurons at the present time except to point out that it is unlikely that Kv1.2, which is insensitive to low concentrations of TEA, is present as a homomeric channel in our studies where all the current was blocked by a low concentration of TEA. Furthermore, it has been reported that the specific Kv1.1 antagonist, Toxin K, can confer sensitivity to a non-sensitive channel with only one subunit of Kv1.1 present in a hetero-multimer (Wang *et al.* 1999). Thus, it is likely that Kv1.2 and/or Kv1.6 underlie the current that is not blocked by Toxin K.

Model explorations of a functional role for the Kv1.1, Kv1.2 and Kv1.6 channels

The composite of ionic currents expressed by a neuron is designed to support its function and, therefore, differences among groups of neurons are expected. For instance, the profile of K^+ current of visceral sensory neurons designed to code and transmit information to the brainstem from the peripheral terminals is quite different from that of spontaneously active integrative brainstem neurons upon which the sensory neurons terminate (Moak & Kunze, 1993; Schild *et al.* 1993). A major impetus for this study was to define potassium channels that contribute to the stabilization of membrane potential of the sensory neuron. In a previous study, we developed membrane models of A- and C-type sensory neurons to reveal the role of the ionic currents underlying the resting potential, action potential wave shape and discharge in response to sustained depolarization (Schild *et al.* 1994). In the present study we used this original model formulation but included mathematical expressions for the voltage-dependent characteristics of the α-DTX-sensitive current (I_{dtx}), removing it from the $I_{4\text{-}AP}$. The model, together with the electrophysiological studies, helps provide a cellular basis for interpreting the recent data arising from studies of the Kv1.1 null mouse (Smart *et al.* 1998; see below).

Role of I_{dtx} in resting and action potentials

Both A- and C-type nodose neurons exhibited resting potentials well below the activation of I_{dtx} near −45 mV. More positive than this level, removal of I_{dtx} resulted in a modest depolarization consistent with the activation characteristics of this current. At membrane voltages near threshold and over the initial phases of the action potential, I_{dtx} functioned to limit depolarization and accelerate repolarization much in the same manner as the other rapidly activating outward K^+ currents. Thus, removal of I_{dtx} permitted a more rapid charging of membrane capacitance toward the threshold for action potential discharge. Such an effect was apparent in both the A- and C-type populations of nodose neurons.

Removal of I_{dtx} had a small effect on the action potential wave shape and the impact was only slightly greater in C-type than in A-type neurons. The model results indicated that A-type action potentials changed less upon removal of I_{dtx} than C-type action potentials because of the large contribution the transient outward current, $I_{4\text{-}AP}$, makes to the total outward K^+ current in A-type neurons. In C-type neurons the slower upstroke velocity combined with the delayed repolarization or hump brought about by the TTX-resistant Na^+ current afforded more time for the transient component of the 4-AP-sensitive current to inactivate. The net effect was that the complement of K^+ currents could not respond sufficiently to compensate for the loss of I_{dtx} and thus C-type action potentials tended to broaden.

An examination of the total K^+ currents under control conditions demonstrated how the α-DTX-sensitive current contributed to the total outward K^+ current over the course of an action potential. The α-DTX-sensitive current exhibited activation characteristics (Figs 4 and 7) that are considerably faster than I_K and $I_{K,Ca}$ and rival those of the transient component of the $I_{4\text{-}AP}$ current. As a result, over the course of the action potential upstroke, I_{dtx} activates to a greater extent than these slower K^+ currents. The data clearly demonstrate that with the removal of I_{dtx} there are changes in discharge and action potential wave shape, but not to such an extent that the action potential is greatly distorted or that the cell fails to repolarize. This happens because the contribution of the remaining K^+ currents increases to compensate for the loss of I_{dtx}. A-type neurons have a large 4-AP-sensitive component that increases with the loss of the α-DTX-sensitive current (Fig. 11*B*). Because the time-dependent characteristics of the 4-AP-sensitive current closely follow those of the α-DTX-sensitive current there are no dramatic changes in the action potential wave shape. C-type neurons have a much smaller 4-AP-sensitive component, with $I_{K,Ca}$ playing a more prominent role in repolarization. The $I_{K,Ca}$ also increases to compensate for the loss of I_{dtx} (Fig. 11*D*). However, since the time-dependent characteristics of $I_{K,Ca}$ are slower than those of I_{dtx}, the rate of repolarization is somewhat slower and the action potential broadens. These dynamic features, while observed in our data as changes in action potential wave

shape, cannot be easily dissected experimentally. The data presented in Fig. 11 and the conclusion drawn from it remain as model predictions.

Role of I_{dtx} in producing repetitive discharge

The most notable change in the presence of α-DTX was in the excitability of the neurons. In the C-type cells and the model, current steps typically elicited a single or short burst of action potentials that changed into longer discharge periods with increasing stimulus current. A similar response pattern was observed upon removal of I_{dtx} but, at all stimulus intensities, either longer bursts or greater discharge rates were observed when compared to control traces. For A-type cells, the impact of I_{dtx} upon discharge was less pronounced, with only a slight increase in discharge rate upon removal of I_{dtx}. Since the depth and time course of the AHP directly impacts the rate and character of repetitive discharge, these results were consistent with the change in the peak AHP upon removal of I_{dtx} in C-type compared with A-type cells. As the AHP traverses membrane voltages that are below the activation threshold for I_{dtx} the manner in which this current deactivates becomes critically important. Around −60 mV the time constant for deactivation (or 'activation' for the two-state model used here) was approximately 15 ms. This rate was slow enough to make I_{dtx} one of the larger K^+ currents over the initial phase of the AHP in both the A- and C-type neuron models. This implied that removal of I_{dtx} would elevate discharge in both A- and C-type neurons, but the data show α-DTX to have a greater effect on C-type discharge than on A-type. The model indicated that such functional differences arose from the relative contributions of I_{dtx}, $I_{4\text{-}AP}$, $I_{K,Ca}$ and I_K to the total outward K^+ current. In A-type neurons I_{dtx} and, to a lesser extent, $I_{4\text{-}AP}$, $I_{K,Ca}$ and I_K all contributed over the full time course of the AHP. As membrane voltage returned toward resting potentials at the end of the AHP, I_K and $I_{4\text{-}AP}$ were recruited. Removal of I_{dtx} accelerated membrane depolarization over the later phase of the AHP but the presence of a large $I_{4\text{-}AP}$ meant that sufficient compensatory current could be rapidly generated along with somewhat smaller increases in $I_{K,Ca}$ and I_K (compare Fig. 11*A* and *B*). In C-type neurons I_{dtx}, $I_{K,Ca}$, I_K and, to a much lesser extent, $I_{4\text{-}AP}$ contributed over the full time course of the AHP. The voltage- and time-dependent properties of $I_{K,Ca}$ and I_K were such that these currents could not compensate for the loss of I_{dtx}.

Based on the present study, we propose that α-DTX-sensitive currents serve to limit the excitability of the soma following action potential invasion from the periphery. Under physiological conditions, following invasion by an action potential from the periphery, the membrane potential of the soma would be expected to return quickly to levels more negative than the activation range of the α-DTX-sensitive currents, perhaps without need for the α-DTX-sensitive current. However, recent studies in dorsal root ganglion sensory neurons provide evidence for cross-excitation that leads to depolarization of adjacent neurons (Amir & Devor, 2000). The source of the excitation may be activity-dependent accumulation of extracellular potassium or non-synaptically released transmitters. Furthermore, it has been demonstrated that cultured sensory neurons release neuropeptides such as substance P from the soma (MacLean *et al.* 1990) and vesicular release from the soma has also been demonstrated (Hay & Hasser, 1998). These transmitters might be expected to diffuse to adjacent cells and even activate autoreceptors on the releasing cell. The presence of α-DTX-sensitive currents under these depolarizing conditions may prevent repetitive discharge, stabilizing the resting potential. This is concordant with the general theme that is developing for the role of the α-DTX-sensitive channels, as explored recently in transgenic mice lacking Kv1.1. The absence of Kv1.1 causes hippocampal CA3 neurons to display increased excitability under conditions that would be expected to produce a depolarization that brings the membrane potential closer to the range where Kv1.1 is activated (such as raising extracellular K^+ or blocking inhibitory input; Smart *et al.* 1998). Our experimental and modelling results are consistent with and provide explanations for these observations.

REFERENCES

Agostoni, E., Chinnock, J. E., DeBurgh Daly, M. & Murray, J. G. (1957). Functional and histological studies of the vagus nerve and its branches to the heart, lungs and abdominal viscera in the cat. *Journal of Physiology* **135**, 182–205.

Amir, R. & Devor, M. (2000). Functional cross-excitation between afferent A- and C-neurons in dorsal root ganglia. *Neuroscience* **95**, 189–195.

Belmonte, C. & Gallego, R. (1983). Membrane properties of cat sensory neurones with chemoreceptor and baroreceptor endings. *Journal of Physiology* **342**, 603–614.

Bertoli, A., Moran, O. & Conti, F. (1994). Activation and deactivation properties of rat brain K channels of the Shaker-related family. *European Biophysical Journal* **23**, 379–384.

Christie, M. J., Adelman, J. P., Douglass, J. & North, R. A. (1989). Expression of a cloned rat brain potassium channel in xenopous oocytes. *Science* **244**, 221–224.

Christie, M. J., North, R. A., Osborne, P. B., Douglass, J. & Adelman, J. P. (1990). Heteropolymeric potassium channels expressed in *Xenopus* oocytes from cloned subunits. *Neuron* **4**, 405–411.

D'Adamo, M. C., Imbrici, P., Sponcichetti, F. & Pessia, M. (1999). Mutations in the KCNA1 gene associated with episodic ataxia type-1 syndrome impair heteromeric voltage gated K channel function. *FASEB Journal* **13**, 1335–1345.

Devor, M. (1999). Unexplained peculiarities of the dorsal root ganglion. *Pain Supplement* **6**, S27–S35.

Ducreux, C., Reynaud, J. C.& Puizillout, J. J. (1993). Spike conduction properties of T-shaped C neurons in the rabbit nodose ganglion. *Pflügers Archiv* **424**, 238–244.

Evans, D. H. L. & Murray, J. G. (1954). Histological and functional studies on the fibre composition of the vagus nerve of the rabbit. *Journal of Anatomy* **88**, 320–337.

Gallego, R. & Eyzaguirre, C. (1978). Membrane and action potential characteristics of A and C nodose ganglion cells studied in whole ganglia and in tissue slices. *Journal of Neurophysiology* **41**, 1217–1232.

Gomez-Hernandez, J. M., Lorra, C., Pardo, L. A., Stuhmer, W., Pongs, O., Heinemann, S. H. & Elliott, A. A. (1997). Molecular basis for different pore properties of potassium channels from the rat brain Kv1 gene family. *Pflügers Archiv* **434**, 661–668.

Grissmer, S., Nguyen, A. N., Aiyar, J., Hanson, D. C., Mather, R. J., Gutman, G. A., Karmilowicz, M. J., Auperin, D. D. & Chandy, K. G. (1994). Pharmacological characterization of five cloned voltage gated K channels, types Kv1.1, 1.2, 1.3, 1.5, 3.1, stably expressed in mammalian cell lines. *Molecular Pharmacology* **45**, 1227–1234.

Grupe, A., Schroter, K. H., Ruppersberg, J. P., Stocker, M., Drewes, T., Beckh, S. & Pongs, O. (1990). Cloning and expression of a human voltage-gated potassium channel. A novel member of the RCK K^+ channel family. *EMBO Journal* **9**, 1749–1756.

Harvey, A. L. (1997). Recent reviews on dendrotoxins and potassium channels. *General Pharmacology* **28**, 7–12.

Hay, M. & Hasser, E. M. (1998). Measurement of synaptic vesicle exocytosis in aortic baroreceptor neurons. *American Journal of Physiology* **275**, H710–716.

Hoffman, H. H. & Kuntz, A. (1957). Vagus nerve components. *Anatomical Record* **127**, 551–567.

Hopkins, W. F. (1998). Toxin and subunit specificity of blocking affinity of three peptide toxins for heteromultimeric, voltage-gated potassium channels expressed in *Xenopus* oocytes. *Journal of Pharmacology and Experimental Therapeutics* **285**, 1051–1060.

Hopkins, W. F., Allen, M. L., Houamed, K. M. & Tempel, B. L. (1994). Properties of voltage-gated K^+ currents expressed in *Xenopus* oocytes by mKv1.1, mKv1.2 and their heteromultimers as revealed by mutagenesis of the dendrotoxin-binding site in mKv1.1. *Pflügers Archiv* **428**, 382–390.

Jaffe, R. A. & Sampson, S. R. (1976). Analysis of passive and active electrophysiologic properties of neurons in mammalian nodose ganglia maintained in vitro. *Journal of Neurophysiology* **39**, 802–815.

Kirsch, G. E., Drewe, J. A., Vermam, S., Brown, A. M. & Joho, R. H. (1991). Electrophysiological characterization of a new member of the RCK family of rat brain K^+ channels. *FEBS Letters* **278**, 55–60.

Klumpp, D. J., Farber, D. B., Bowes, C., Song, E. J. & Pinto, L. H. (1991). The potassium channel MBK1 (Kv1.1). is expressed in the mouse retina. *Cell and Molecular Neurobiology* **11**, 611–622.

Kuryshev, Y. A., Wible, B. A., Gudz, T. I., Ramirez, A. N. & Brown, A. M. (2001). KChAP/Kvβ1.2 interactions and their effects on cardiac Kv channel expression. *American Journal of Physiology* **281**, C290–299.

Lieberman, A.R. (1976). *Sensory Ganglia in the Peripheral Nerve*, ed. Landon, D. N., pp. 188–278. Chapman and Hall, London.

MacLean, D. B., Wheeler, F. & Hayes, L. (1990). Basal and stimulated release of substance P from dissociated cultures of vagal sensory neurons. *Brain Research* **519**, 308–314.

Moak, J. & Kunze, D. L. (1993). Potassium currents of neurons isolated from medial nucleus tractus solitarius in guinea pig. *American Journal of Physiology* **265**, H1596–1602.

Moran, O. & Conti, F. (1995). Properties of the Kv1.1 rat brain potassium channels expressed in mammalian cells: temperature effects. *Biochemical and Biophysical Research Communications* **215**, 915–920.

Robertson, B., Owen, D., Stow, J., Butler, C. & Newland, C. (1996). Novel effects of dendrotoxin homologues on subtypes of mammalian Kv1 potassium channels expressed in *Xenopus* oocytes. *FEBS Letters* **383**, 26–30.

Schild, J. H., Clark, J. W., Hay, M., Mendelowitz, D., Andresen, M. C. & Kunze, D. L. (1994). A and C type nodose sensory neurons: Model interpretations of dynamic discharge characteristics. *Journal of Neurophysiology* **71**, 2338–2358.

Schild, J. H., Khushalani, J., Clark, J. W., Andresen, M. C., Kunze, D. L. & Yang, M. (1993). An ionic current model for neurons in the rat medial nucleus tractus solitarius receiving sensory afferent input. *Journal of Physiology* **469**, 341–363.

Schild, J. H. & Kunze, D. L. (1997). Kinetic diversity of the TTX-resistant Na^+ current underlies the heterogeneous discharge properties of C-type nodose neurone in the rat. *Journal of Neurophysiology* **78**, 3198–3209.

Smart, S. L., Lopantsev, V., Zhang, C. L., Robbins, C. A., Wang, H., Chiu, S. Y., Schwartzkroin, P. A., Messing, A. & Tempel, B. L. (1998). Deletion of the Kv1.1 potassium channel causes epilepsy in mice. *Neuron* **20**, 809–819.

Sprunger, L. K., Stewig, N. J. & O'Grady, S. M. (1996). Effects of charybdotoxin on K^+ channel (KV1.2) deactivation and inactivation kinetics. *European Journal of Pharmacology* **314**, 357–364.

Stansfeld, C. E., Marsh, S. J., Halliwell, J. V. & Brown, D. A. (1986). 4-Aminopyridine and dendrotoxin induce repetitive firing in rat visceral sensory neurones by blocking a slowly inactivating outward current. *Neuroscience Letters* **64**, 299–304.

Stansfeld, C. E. & Wallis, D. I. (1985). Properties of visceral primary afferent neurons in the nodose ganglion of the rabbit. *Journal of Neurophysiology* **54**, 245–260.

Stuhmer, W., Ruppersberg, J. P., Schoerter, K. H., Sakmann, B., Socker, M., Geise, K. P., Perschke, A., Baumann, A. & Pongs, O. (1989). Molecular basis of functional diversity of voltage-gated potassium channels in mammalian brain. *EMBO Journal* **8**, 3235–3244.

Wang, F. C., Parcej, D. N. & Dolly, J. O. (1999). Alpha subunit compositions of Kv1.1-containing K^+ channel subtypes fractionated from rat brain using dendrotoxins. *European Journal of Biochemistr y* **263**, 230–237.

Wang, H., Kunkel, D. D., Martin, T. M., Schwartzkroin, P. A. & Tempel, B. L. (1993). Heteromultimeric K^+ channels in terminal and juxtaparanodal regions of neurons. *Nature* **365**, 75–79.

Wang, Q., Wang, L. & Wardwell-Swanson, J. (1998). Modulation of cloned human neuronal voltage-gated potassium channels (hKv1.1 and hKv2.1) by neurosteroids. *Pflügers Archiv* **437**, 49–55.

Authors' present addresses

T. Doan: Department of Pathology and Laboratory Medicine, Emory University, Atlanta, GA 30322, USA.

C.-C. Shieh: Neurological and Urological Diseases Research, Department 47C, Building AP9A, Abbott Laboratories, 100 Abbott Park Road, Abbott Park, IL 60064-6125, USA.